Forward-Compatible Integrated Sensing and Communication for WiFi

Yinghui He, *Member, IEEE,* Jianwei Liu, *Student Member, IEEE,* Mo Li, *Fellow, IEEE,* Guanding Yu, *Senior Member, IEEE,* and Jinsong Han, *Senior Member, IEEE*

***Abstract*—Given the fact that WiFi-based sensing can be realized through the reuse of WiFi communication facilities and frequency bands, integrated sensing and communication (ISAC) emerges as a pivotal direction for future WiFi standards, such as IEEE 802.11bf. Traditional WiFi sensing systems extract channel state information (CSI) from exclusive WiFi packets to quantify the characteristics of the sensing target. This poses challenges for existing WiFi systems originally designed for communication purposes, as it demands high-quality and sufficient CSI measurements. In this paper, we propose *SenCom* as a step towards forward-compatible ISAC solution. *SenCom* extracts CSI from general WiFi packets, enabling CSI calibration across different WiFi communication modes and delivering quality CSI measurements for upper-layer sensing applications. A fitting-resampling scheme and an incentive strategy are also developed. The former one is to obtain evenly sampled CSI with consistent dimensionality and the latter one is to guarantee sufficient CSI measurements over time. We build a prototype of *SenCom* and conduct extensive experiments involving 15 participants. The results show that *SenCom*'s competence for a variety of sensing tasks while making minimal compromises to WiFi communication performance.**

***Index Terms*—Integrated sensing and communication, WiFi sensing, channel state information, forward compatibility**

I. Introduction

Recent studies [2]–[4] have demonstrated the feasibility of non-intrusive sensing using a wide range of wireless radio frequency (RF) signals, with WiFi standing out due to its widespread deployment [5]. Unfortunately, most existing WiFi sensing approaches are dependent on specific radio configurations and specialized purposed probing packets for detecting channel variations. This approach disrupts WiFi's primary function as a means of communication. In this paper, we explore a system solution to such a problem - enabling forward-compatible integrated sensing and communication (ISAC) [6]–[8] in practice without compromising the state-of-the-art communication capabilities of WiFi.

Rather than seeking additional spectrum usage or relying on exclusive transmissions for sensing (Fig. 1(a)), our solution maximizes the utilization of existing in-band WiFi communication traffic without introducing extra overhead. Such a goal is hard to achieve as high-performance WiFi sensing demands quality and sufficiency in channel state information (CSI), presenting the following challenges. (i) Advanced WiFi standards like 802.11n/ac/ax [9] supports multiple-input multiple-output (MIMO) communications [10], alternating between diversity and multiplexing modes. These two modes possess different mapping matrices for different numbers of data streams. The measured CSI cannot be directly translated to channel coefficients for sensing the object dynamics without knowing the specific MIMO setting. (ii) WiFi's use of beamforming [11] to enhance signals directed at communication clients may weaken signals reflected from the sensing target, resulting in a low sensing signal-to-noise ratio (SNR) that degrades sensing performance. (iii) General WiFi transmissions are unevenly distributed in time due to varying communication demands, leading to insufficient packets to probe the channel at times, disabling the sensing. As demonstrated by our experiments in Section VI, directly using non-unified CSI measured from communication packets (the first and second challenges) would lead to 15% accuracy reduction for activity recognition, while using communication packets only (the third challenge) is often not enough for sensing at all, e.g., when the client is running online games.

In this paper, we address the above challenges and propose *SenCom*, to the best of our knowledge, the first practical ISAC system that enables seamless WiFi sensing with general communication traffic. As shown in Fig. 1(b), *SenCom* can be implemented on one normal WiFi client and sniff the ongoing WiFi transmissions between the WiFi AP and clients (including the client with *SenCom*). *SenCom* measures the CSI from all packets transmitted by the WiFi AP, making full use of the existing communication packets, and derives the environment dynamics for various sensing tasks based on that. In such a way, there is no disruption to any of the ongoing WiFi communication flows between the AP and clients.

Manuscript received October 30, 2023; revised March 18, 2024 and April 20, 2024; accepted May 8, 2024. This work is supported by the National Natural Science Foundation of China under grant U21A20462 and 62372400, "Pioneer" and "Leading Goose" R&D Program of Zhejiang under grant No. 2024C03287. Part of this paper was presented at MobiCom'23 [1]. *(Yinghui He and Jianwei Liu contribute equally to this work.) (Corresponding authors: Guanding Yu and Jinsong Han.)*

Y. He is with the College of Information Science and Electronic Engineering, Zhejiang University, Hangzhou 310027, China, and also with the College of Computing and Data Science, Nanyang Technological University, 639798, Singapore (e-mail: 2014hyh@zju.edu.cn).

J. Liu is with the College of Computer Science and Technology, Zhejiang University, Hangzhou 310027, Zhejiang, China, and also with the School of Information and Electrical Engineering, Hangzhou City University, Hangzhou 310015, China (e-mail: jianweiliu@zju.edu.cn).

M. Li is with the Department of Computer Science and Engineering, The Hong Kong University of Science and Technology, Hong Kong (e-mail: lim@cse.ust.hk).

G. Yu is with Wenzhou Key Laboratory for Intelligent Networking, Wenzhou University, Wenzhou 325035, China, and also with the College of Information Science and Electronic Engineering, Zhejiang University, Hangzhou 310027, Zhejiang, China (e-mail: yuguanding@zju.edu.cn).

J. Han is with the College of Computer Science and Technology, Zhejiang University, Hangzhou 310027, Zhejiang, China (e-mail: hanjinsong@zju.edu.cn).

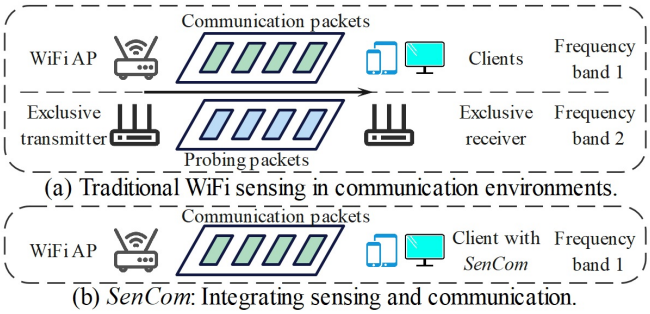

Fig. 1. Comparing traditional WiFi sensing with our ISAC solution-*SenCom*.

Specifically, we conduct a comprehensive analysis of various MIMO transmission modes, culminating in the derivation of a transformation formula. This formula can transform the collected CSI data from different transmission modes into a unified form. As a result, agnostic sensing applications become achievable using this unified CSI without the knowledge of the specific configurations of each WiFi transmission flow (which is WiFi AP/client-specific and often unknown to the sniffers). We also introduce a compensation formula that enables the reconstruction of potential beamforming steering matrices when considering two feedback types. Based on its inverse, we can suppress the impact of beamforming. In order to address the temporal irregularity of WiFi transmissions, we introduce a fitting-resampling scheme. This scheme is designed to obtain CSI samples with consistent dimensionality, facilitating the mapping and model training of upper-layer sensing applications. Furthermore, we delve into the trade-off between the sensing and communication performance and inject active probing packets (i.e., incentive packets) when the normal WiFi traffic is inadequate, while ensuring minimal disruption to communication.

We implement a prototype of *SenCom* with commercial off-the-shelf (COTS) 802.11ac WiFi devices and conduct real-world experiments involving 15 human participants across three diverse test environments. The experimental results highlight *SenCom*'s ability to effectively support various sensing tasks with quality and sufficient CSI. Post-implementation of *SenCom*, we observed only a modest $\sim$2% reduction in throughput and delay of the communication system. Furthermore, reproducing four existing WiFi sensing applications demonstrates 94.4% accuracy for activity recognition, an error rate of 1.6% for step counting, 97.6% accuracy for person identification, and a rate error lower than 2 beats per minute for respiration monitoring when applying *SenCom* to support ISAC. In summary, our contributions are as follows:

- We propose *SenCom*, the first practical WiFi ISAC system designed for seamless integration into existing communication systems. *SenCom* can be implemented without modifying any existing WiFi communication standards, devices, or settings.
- *SenCom* incorporates a CSI calibration method, featuring a transformation formula to unify CSI data and a compensation formula to mitigate the effects of beamforming. To supply sufficient CSI, *SenCom* adopts a fitting-resampling scheme to support upper-layer sensing applications, as well as an incentive strategy to elicit compensation probing packets where a closed-form incentive rate is derived to balance sensing and communication performance.
- We build a prototype of *SenCom* and conduct real-world experiments on it. Our empirical findings confirm that *SenCom* significantly enhances both the quantity and quality of CSI collected in a communication context, all while having minimal impact on communication throughput and latency. Through case studies on real-world sensing applications, *SenCom* demonstrates its practicability and reliability across a variety of sensing tasks.

TABLE I
COMPARING *SenCom* WITH WU ET AL. [12] AND HU ET AL. [13].

Solution	Robustness to MIMO	Robustness to beamforming	Robustness to CSI deficiency
Wu et al. [12]	×	✓	×
Hu et al. [13]	×	×	✓
SenCom	✓	✓	✓

The rest of the paper is organized as follows. Section II summarizes the related work. Section III presents problem statement and the system overview of *SenCom*. Section IV details the key techniques in CSI calibration. In Section V, we elaborate on the key techniques in CSI fitting, resampling, and packet incentive. Section VI describes the experimental evaluation results. This paper is concluded in Section VII.

II. Related Work

ISAC: Existing ISAC research mainly focuses on devising a special PHY design that is suitable for both communication and sensing. Most existing works require amendments to existing communication systems or protocols. There are two leading solutions: orthogonal resource allocation [14], [15] and unified waveform design [16]–[18]. Besides, there is a future WiFi standard on sensing, namely 802.11bf, which focuses on designing a new WLAN sensing procedure. The above-mentioned designs require modifications to existing communication systems and are not compatible with most existing WiFi APs and devices. Recently, Wu et al. [12] and Hu et al. [13] propose two forward-compatible ISAC solutions. But, they use beamforming feedback packets for sensing and address part of the impact of communication configurations on sensing, i.e., limited beamforming feedback and intermittent packets, respectively. In this work, we propose *SenCom* to achieve fully forward-compatible ISAC scheme that uses all communication packets for sensing and solves the issues caused by the alternation of two modes, beamforming, and intermittent traffic. To show the advantages of *SenCom*, we compare it with the two most related works [12], [13] in terms of the robustness against MIMO, beamforming, and packet deficiency, as shown in Tab. I. One can clearly see that *SenCom* can adapt to all kinds of communication settings and achieve ISAC in existing WiFi systems.

WiFi-based sensing: WiFi has been exploited for various sensing purposes. Existing WiFi-based sensing applications fall into two categories according to the sensing goals: detection/recognition and estimation [6]. Therein, detection and recognition are binary and multi-class classification tasks,

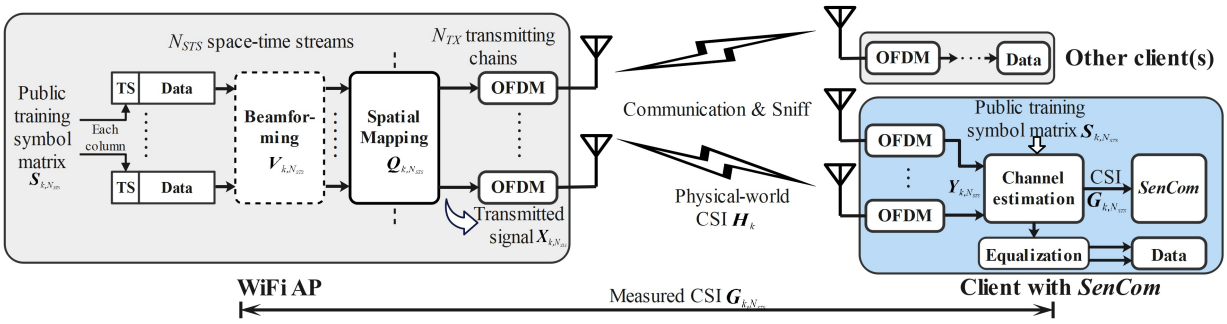

Fig. 2. Signal transmission procedure. 'TS' represents the training symbol vector.

respectively. The second category belongs to the measurement task. Detection systems usually aim at achieving binary sensing tasks, such as human presence detection [13], [19], fall detection [20], and motion detection [21]–[23]. Recognition systems are generally utilized to accomplish multi-class prediction tasks, such as activity recognition [5], gesture recognition [2], user identification [24], and so on. In an estimation system, users can acquire quantitative feedback, such as location [25] and breathing rate [26]. Although a lot of previous works reuse WiFi frequency band and COTS WiFi devices to implement the sensing systems, none of them can directly work with normal WiFi 802.11ac/ax data traffic due to the impact of communication-oriented designs like MIMO and beamforming. In this paper, we design *SenCom* to enable sensing with such WiFi communication context. Particularly, the design of *SenCom* is independent of any specific sensing task. It helps an arbitrary sensing application in acquiring quality and sufficient CSI data with little impact on ongoing normal WiFi communication.

III. Challenge and System Overview

A. Problem and Challenge

In this part, we elucidate the challenges in achieving our proposal, forward-compatible ISAC, in a practical communication context. We start by reviewing the data transmission procedure of the 802.11ac Wave 1 standard [27], which is widely prevalent in current WiFi systems. This procedure utilizes the MIMO technique to enable simultaneous transmissions of multiple data streams (i.e., space-time streams (STSs) [27]) between the WiFi AP and the client, as shown in Fig. 2. To eliminate the unknown channel effect and ensure correct decoding at the client, each data stream sent by the AP has its own training symbol vector, which is instrumental for measuring CSI. All training symbol vectors of N_{STS} STSs form a training symbol matrix. CSI is passively measured by a monitor, like *SenCom*, based on the sniffed training symbol matrix. Specifically, before being transmitted by the antennas, the training symbol matrix undergoes three essential processes. (i) When beamforming and directional transmission are needed, the training symbol matrix first passes the steering matrix. (ii) The number of data streams may differ from that of transmitting antennas. Thus, a mapping matrix is necessary to map the N_{STS} data streams to N_{TX} transmitting chains for subsequent transmission. (iii) To avoid inter-code interference, orthogonal frequency division multiplexing (OFDM) modulation [28] is employed, dividing wireless bandwidth into K subcarriers for parallel transmission. Let $\boldsymbol{S}_{k,N_{STS}} \in \mathbb{C}^{N_{STS}\times N_{STS}}$ be the training symbol matrix of N_{STS} STSs for subcarrier k, with each row of $\boldsymbol{S}_{k,N_{STS}}$ corresponding to the training symbol vector for each data stream and $\mathbb{C}$ representing the set of complex numbers. The final transmitted signal at the WiFi AP for subcarrier k can be expressed by:

$$\boldsymbol{X}_{k,N_{STS}} = \boldsymbol{Q}_{k,N_{STS}} \boldsymbol{V}_{k,N_{STS}} \boldsymbol{S}_{k,N_{STS}}, \tag{1}$$

where $\boldsymbol{Q}_{k,N_{STS}} \in \mathbb{C}^{N_{TX}\times N_{STS}}$ and $\boldsymbol{V}_{k,N_{STS}} \in \mathbb{C}^{N_{STS}\times N_{STS}}$ are the mapping matrix and the steering matrix for potential beamforming, respectively. When $N_{STS} = 1$, the transmitter works in the diversity mode; otherwise, the transmitter works in the multiplexing mode.

After undergoing the physical-world wireless channel, denoted by $\boldsymbol{H}_k \in \mathbb{C}^{N_{RX}\times N_{TX}}$ for subcarrier k, and OFDM demodulation, the signal measured at *SenCom* is:

$$\begin{aligned}\boldsymbol{Y}_k &= \boldsymbol{H}_k \boldsymbol{X}_{k,N_{STS}} + \boldsymbol{N}_0 \\ &= \boldsymbol{H}_k \boldsymbol{Q}_{k,N_{STS}} \boldsymbol{V}_{k,N_{STS}} \boldsymbol{S}_{k,N_{STS}} + \boldsymbol{N}_0,\end{aligned} \tag{2}$$

where $\boldsymbol{N}_0 \in \mathbb{C}^{N_{RX}\times N_{STS}}$ is the Gaussian white noise with N_{RX} being the number of the receiving antennas. As shown in Fig. 2, CSI can be calculated from $\boldsymbol{Y}_k$ at the monitor with the public training symbol matrix. As the monitor lacks awareness of the transmitting configurations at the AP side, it perceives the received signal at each receiving antenna as a superimposed signal, akin to a signal traversing a steered wireless channel from a "virtual antenna". The measured CSI can be represented as follows:

$$\boldsymbol{G}_{k,N_{STS}} = \boldsymbol{H}_k \boldsymbol{Q}_{k,N_{STS}} \boldsymbol{V}_{k,N_{STS}}. \tag{3}$$

$\boldsymbol{G}_{k,N_{STS}}$ characterizes the channel between the virtual antennas and receiving antennas at the monitor. It is subject to the influences of the MIMO and beamforming techniques, which makes it distinct from the physical-world CSI $\boldsymbol{H}_k$. The latter characterizes the physical-world channel between the transmitting antennas and receiving antennas.

Challenge 1-Qualified CSI. As the monitor passively sniffs the WiFi traffic between the AP and clients, it operates without knowledge of the MIMO and beamforming configurations employed at the AP. This raises two problems. First, the AP's operation mode - diversity or multiplexing - depends on the client's demands, and this mode switching is unpredictable for a passive monitor like *SenCom*. Consequently,

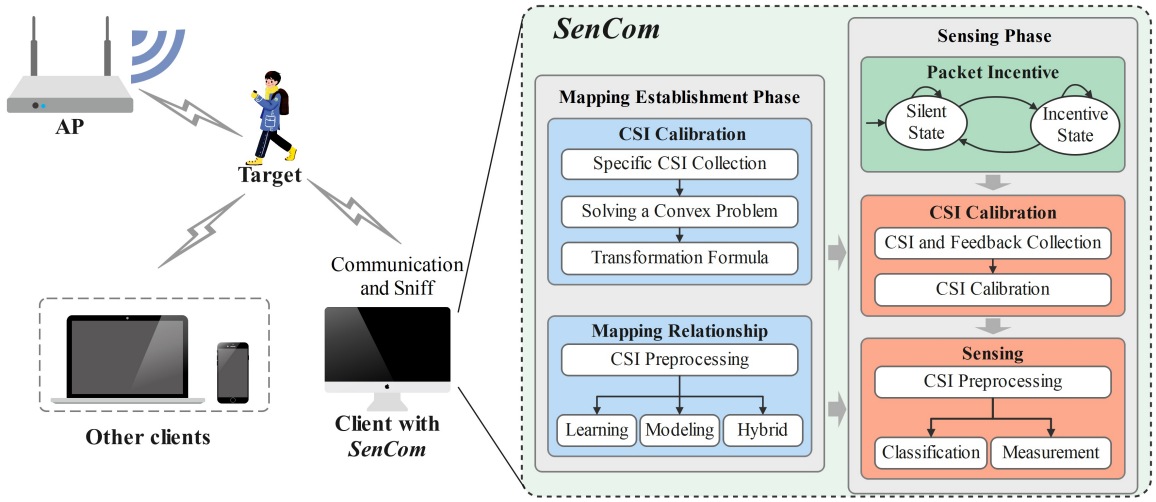

Fig. 3. Architecture of *SenCom*.

the monitor lacks awareness of the operational mode of the AP. Unfortunately, the CSI collected under different modes differs even when the actual physical environment remains unchanged (as indicated in Eq. 3). This divergence means that a sensing model established under one mode cannot function optimally under the other. Thus, the monitor *remains agnostic regarding which mode's sensing model to use.* Furthermore, beamforming introduces directional transmission. This may *result in a weakened signal towards the sensing target and thus impair the SNR of the collected CSI*, hindering the derivation of accurate sensing results. Our design has to compensate for such an effect.

Challenge 2-Sufficient CSI. WiFi sensing relies on a sufficient amount of CSI related to the sensing target. Traditional WiFi sensing systems achieve this by configuring the AP to send probing packets at regular and short time intervals [2] (usually less than 20 ms). In the considered ISAC context, however, the transmitter (e.g., AP) sends packets based only on the communication requirements of the connected clients. These clients may have sporadic downlink traffic needs, resulting in unevenly distributed data transmissions that might occasionally prove insufficient for sensing purposes. Our design has to adapt to practical WiFi systems, transform the sampled CSI into the evenly-distributed one, and trigger extra probing packets when necessary.

B. System Overview

As shown in Fig. 3, *SenCom* collects CSI of the wireless channel from the AP by sniffing its transmissions to various clients. *SenCom*'s operation unfolds in two main phases: *mapping establishment phase* and *sensing phase*.

During *mapping establishment phase*, *SenCom* engages in CSI pre-calibration and establishes a mapping relationship between the CSI and the sensing objective. To accomplish CSI calibration, *SenCom* must gather CSI data in two distinct modes by accessing the AP. Subsequently, relying on the collected CSI, *SenCom* derives a pivotal transformation matrix that unifies the CSI. Following this, *SenCom* undertakes a sequence of potential preprocessing steps, such as fitting-resampling, on the calibrated CSI to facilitate upper-layer applications. Applications can be realized by establishing a mapping relationship (modeling-based, learning-based, or hybrid [6]) connecting the CSI to the sensing objective.

In *sensing phase*, *SenCom* conducts sensing tasks using the pre-established mapping relationship, while the incentive strategy remains running to ensure an adequate CSI supply. Specifically, *SenCom* first collects the CSI samples along with feedback on beamforming from the clients. With the pre-acquired transformation formula and a compensation formula for suppressing the impact of beamforming, the collected CSI samples can be calibrated into a unified form. The same preprocessing techniques employed in the *mapping establishment phase* are then applied to the CSI samples. Given that WiFi-based sensing can be either classification-driven or measurement-driven, the pre-processed CSI data is fed into the mapping relationship to perform classification or measurement tasks.

IV. CSI Calibration

This section shows a CSI calibration method for mitigating the negative effects of particular communication designs, i.e., MIMO and beamforming, on the sensing performance.

A. CSI Transformation

Having multiple transmitting antennas allows the AP to use either the diversity mode or multiplexing mode to achieve specific communication purposes. This presents the first challenge outlined in Section I. In this part, we commence by revisiting the experssion of CSI in Eq. 3 to better understand the origins of this challenge. For the sake of clarity, we will take a two-antenna AP as an example and consider that *SenCom* has one receiving antenna. We will explore the disparities between the CSI collected in the two modes and detail how to transform the CSI from the multiplexing mode to that of the diversity mode. Note that we do not take beamforming into account, as that aspect will be addressed in the subsequent subsection.

1) CSI Discrepancy Between Two Modes: In the diversity mode, there is only one data stream ($N_{STS} = 1$). It occurs when the client has only one antenna or when stability is

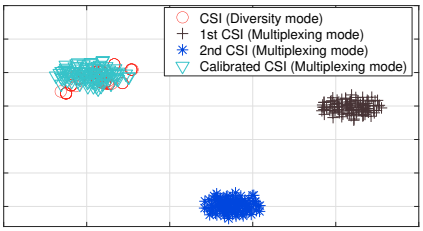

Fig. 4. CSI distribution under diversity mode is different from that under multiplexing mode. Our calibration method can unify the CSI distribution.

prioritized over high throughput. Only one training symbol s_k is allocated to the data stream for subcarrier k, that is, $\boldsymbol{S}_{k,N_{STS}}$ in Fig. 2 becomes s_k when $N_{STS} = 1$. Subsequently, the training symbol is mapped into two transmitting chains with a mapping matrix $\boldsymbol{Q}_{k,1} = [q_{k,1}, q_{k,2}]^T$. The symbols in these two transmitting chains are $x_{k,1} = q_{k,1}s_k$ and $x_{k,2} = q_{k,2}s_k$, respectively. After traversing the wireless channel $\boldsymbol{h}_k = [h_{k,1}, h_{k,2}]$ between the AP and *SenCom*, the received signal at *SenCom* is y_k. In this case, *SenCom* can only 'see' one virtual transmitting antenna rather than two real ones. This limitation arises because the AP sends only one training symbol, and the signals from the two real transmitting antennas become superimposed. The measured CSI between the virtual transmitting antenna and the receiving antenna is:

$$g_{k,1} = \boldsymbol{h}_k \boldsymbol{Q}_{k,1}. \tag{4}$$

In this mode, the physical-world CSI $\boldsymbol{h}_k$ between the AP and *SenCom* is transformed into $g_{k,1}$.

In the multiplexing mode, the transmitting process is similar to that in the diversity mode, *with the key distinctions revolving around the training symbol and mapping matrix.* The multiplexing mode uses two training symbol vectors. Meanwhile, the mapping matrix used in the multiplexing mode becomes:

$$\boldsymbol{Q}_{k,2} = \begin{bmatrix} q_{k,1,1} & q_{k,1,2} \\ q_{k,2,1} & q_{k,2,2} \end{bmatrix}.$$

Thus, in the multiplexing mode, after undergoing the wireless channel, *SenCom* can 'see' two virtual transmitting antennas. The measured CSI between the virtual transmitting antennas and the receiving antenna is expressed as:

$$\boldsymbol{g}_{k,2} = \boldsymbol{h}_k \boldsymbol{Q}_{k,2}. \tag{5}$$

Conclusion: As evidenced by Eq. 4 and 5, it is clear that the CSI collected under different modes can exhibit variations even when the environment remains constant. Notably, the diversity mode yields one CSI stream, while the multiplexing mode produces two streams. To visually illustrate such differences, we first collect two batches of CSI samples under these two modes in a static environment. Then, we use the dimensionality reduction algorithm t-SNE [29] to convert each CSI sample into two-dimensional data. Fig. 4 depicts the resultant CSI distributions, where the x-axis and y-axis correspond to the two dimensions of the t-SNE results, respectively. It can be seen that the CSI of the diversity mode is far from that of the multiplexing mode. Meanwhile, the two CSI streams of the multiplexing mode also scatter in different clusters. These two modes demonstrate three distinct CSI distributions. These differences present a challenge in establishing a single mapping relationship that performs effectively in both modes. A straightforward solution is to respectively establish three different mapping relationships for the two modes, enabling *SenCom* to choose the most suitable one based on the AP's operating mode. However, it would require direct communication and coordination between *SenCom* and the AP. Such direct interaction would undermine our core objective of achieving sensing without compromising communication performance.

2) CSI Transformation From Multiplexing to Diversity: We seek to unify the CSI of the two modes into a single distribution, such that only one mapping relationship is required for sensing. To accomplish this, there are two potential ways: i) Extracting physical-world CSI from both the diversity mode and the multiplexing mode. ii) Transforming the CSI of the multiplexing mode into that of the diversity mode. However, in the diversity mode, the physical world CSI $\boldsymbol{h}_k$ cannot be recovered from $g_{k,1}$ via Eq. 4 due to infinite possible combinations for $\boldsymbol{h}_k$. *Consequently, the sole viable solution is to transform the CSI from the multiplexing mode to the diversity mode.*

Such a transformation can be achieved in two steps: (i) recovering the physical-world CSI from the multiplexing mode by multiplying $\boldsymbol{Q}_{k,2}^{-1}$ in both sides of Eq. 5; (ii) transforming the recovered CSI into the diversity mode using Eq. 4. We can derive the transformation formula as:

$$g_{k,1} = \boldsymbol{g}_{k,2} \boldsymbol{P}_k, \tag{6}$$

where $\boldsymbol{P}_k \triangleq \boldsymbol{Q}_{k,2}^{-1}\boldsymbol{Q}_{k,1}$ serves as the transformation matrix from the multiplexing mode to the diversity mode.

Now, the challenge shifts to how to obtain $\boldsymbol{P}_k$. In reality, $\boldsymbol{P}_k$ is unknown to *SenCom* and it cannot be derived through straightforward theoretical calculations. To address this issue, we heuristically take advantage of real CSI and propose an optimization-based method for estimating $\boldsymbol{P}_k$. Specifically, we first noticed that the CSI remains unchanged during the coherence time [30]. Based on this property, as long as in the coherence time, the CSI collected in the diversity mode is consistent with that collected in the multiplexing mode. This consistency presents an opportunity to estimate $\boldsymbol{P}_k$. In particular, we place a two-antenna client (e.g., smartphone) and *SenCom* near the AP to access and 'ping' the AP in the coherence time, respectively. Since the AP works in the multiplexing/diversity mode when communicating with the client/*SenCom*, we can collect CSI samples of the two modes. To enhance the accuracy of the estimated $\boldsymbol{P}_k$, we can collect multiple sets of CSI samples in different environments. Let $\left\{g_{k,1}^{(i,1)}, \boldsymbol{g}_{k,2}^{(i,2)}\right\}$ and I represent the i-th CSI sample pair and the total number of pairs, respectively. Since the CSI is invariant within the coherence time, $\boldsymbol{g}_{k,2}^{(i,2)}\boldsymbol{P}_k$ (from the multiplexing mode) is theoretically equal to $g_{k,1}^{(i,1)}$ (from the diversity mode). We can estimate $\boldsymbol{P}_k$ by solving a least-squares optimization problem: $\min_{\boldsymbol{P}_k} \sum_i \left|\left| g_{k,1}^{(i,1)} - \boldsymbol{g}_{k,2}^{(i,2)}\boldsymbol{P}_k \right|\right|^2$.

Nonetheless, due to the phase error $\Delta\gamma_i$ introduced by the receiver of *SenCom* and varied channel gain, $g_{k,1}^{(i,1)}$, and

$\boldsymbol{g}_{k,2}^{(i,2)}\boldsymbol{P}_k$ are not perfectly identical. Based on the prior investigation [31], phase variation between two CSI samples during the coherence time is caused by the uncertainty in packet boundary detection and $\Delta\gamma_i$ follows a Gaussian distribution with zero mean. Taking into account the phase error and varied channel gain, we establish the following relationship between the CSI samples from the two modes: $\alpha_i g_{k,1}^{(i,1)} = \boldsymbol{g}_{k,2}^{(i,2)}\boldsymbol{P}_k$, where $\alpha_i = |\alpha_i|e^{j\Delta\gamma_i}$ and $|\alpha_i|$ characterizes the variation of channel gain with $\mathbb{E}\left\{|\alpha_i|^2\right\} = 1$. $\boldsymbol{P}_k$ can be estimated by $\min\limits_{\alpha_i,\boldsymbol{P}_k} \sum_i \left|\left|\alpha_i g_{k,1}^{(i,1)} - \boldsymbol{g}_{k,2}^{(i,2)}\boldsymbol{P}_k\right|\right|^2$. However, directly solving the problem will lead to $\alpha_i = 0$ and $\boldsymbol{P}_k = \boldsymbol{0}$. To avoid this issue, we introduce a fractional form to prevent α_i and $\boldsymbol{P}_k$ from being zero. Specifically, we introduce two auxiliary variables $\hat{\boldsymbol{P}}_k$ and $\hat{\alpha}_i$, as

$$\hat{\boldsymbol{P}}_k = \boldsymbol{P}_k / \boldsymbol{P}_k(1,1), \tag{7}$$

$$\hat{\alpha}_i = \alpha_i / \boldsymbol{P}_k(1,1), \tag{8}$$

where $\boldsymbol{P}_k(1,1)$ is the element located in the first row and the first column of $\boldsymbol{P}_k$. Then, we have $\hat{\boldsymbol{P}}_k(1,1) = 1$ and the optimization problem can be reformulated as:

$$\min_{\hat{\alpha}_i,\hat{\boldsymbol{P}}_k} \quad \sum_i \left|\left|\hat{\alpha}_i g_{k,1}^{(i,1)} - \boldsymbol{g}_{k,2}^{(i,2)}\hat{\boldsymbol{P}}_k\right|\right|^2, \tag{9a}$$

$$\text{s.t.} \quad \hat{\boldsymbol{P}}_k(1,1) = 1. \tag{9b}$$

This problem is convex, as it is a quadratic optimization problem, and can be solved using existing solvers such as CVX [32]. Importantly, the optimal solution would not yield zero since $\hat{\boldsymbol{P}}_k(1,1)$ is constrained to equal 1.

After obtaining the optimal solution to the problem in Eq. 9, we need to obtain $P_k(1,1)$ for calculating $\boldsymbol{P}_k$. Recalling that the channel gain variation follows $\mathbb{E}\left\{|\alpha_i|^2\right\} = 1$, and thus we have

$$\mathbb{E}\left\{\left|\hat{\alpha}_i \hat{\boldsymbol{P}}_k(1,1)\right|^2\right\} = 1. \tag{10}$$

Then, $P_k(1,1)$ can be estimated as:

$$P_k(1,1) = \sqrt{\frac{1}{I}\sum_{i=1}^{I}|\hat{\alpha}_i|^2} e^{-j\frac{1}{I}\sum_{i=1}^{I}\angle\hat{\alpha}_i}, \tag{11}$$

where $\angle\hat{\alpha}_i$ represents the phase of $\hat{\alpha}_i$. Ultimately, the transformation matrix $\boldsymbol{P}_k$ can be estimated by $\boldsymbol{P}_k = P_k(1,1)\hat{\boldsymbol{P}}_k$. In this way, all the collected CSI can be unified into one mode/distribution using estimated $\boldsymbol{P}_k$. As shown in Fig. 4, the CSI transformed from the multiplexing mode and that of the diversity mode lies in the same cluster. This demonstrates that they have the same distribution and our transformation is very effective. *Note that, since $\boldsymbol{Q}_{k,1}$ and $\boldsymbol{Q}_{k,2}$ are independent of the wireless channel and only related to the AP, the transformation matrix $\boldsymbol{P}_k$ only depends on the AP also. Therefore, $\boldsymbol{P}_k$ can be permanently used across time and environments once it was estimated.*

B. Compensation for Beamforming

Principle of beamforming. This part focuses on beamforming, which is employed in WiFi 802.11ac/ax to enhance communication throughput. In the transmission procedure with beamforming, the AP first sends a null data packet (NDP) to the client before data transmission. Then, the client measures the CSI, denoted by $\boldsymbol{H}_k^c$ for subcarrier k, and provides feedback to the AP. The AP uses this feedback to generate a steering matrix $\boldsymbol{V}_{k,N_{STS}}$ to enable the directional transmission towards the client. *However, when viewed from the perspective of SenCom, the signal's strength passing through the sensing area may become much weaker compared to other regions, resulting in a decrease in the SNR of the CSI.* Thus, we need to mitigate the impact of beamforming, as described below.

Suppressing the impact of beamforming. According to Eq. 3, we need to eliminate the steering matrix $\boldsymbol{V}_{k,N_{STS}}$ in the collected CSI by the following compensation formula:

$$\boldsymbol{G}_{k,N_{STS}}\boldsymbol{V}_{k,N_{STS}}^{-1} = \boldsymbol{H}_k\boldsymbol{Q}_{k,N_{STS}}. \tag{12}$$

We cannot directly apply this formula because the steering matrix $\boldsymbol{V}_{k,N_{STS}}$ is unknown to a passive monitor like *SenCom*. Fortunately, *SenCom* can listen to the feedback of NDP as it is used for creating $\boldsymbol{V}_{k,N_{STS}}$. Here are two feedback types: *uncompressed beamforming feedback* and *compressed beamforming feedback*. Note that We can distinguish these feedback types based on the control field of the feedback.

Under uncompressed beamforming feedback, the measured CSI at the client (i.e., $\boldsymbol{H}_k^c$) is directly fed back to the AP. Here, we mainly consider the case where the sniffed packets are from the clients without implementing *SenCom*, as the obtained $\boldsymbol{H}_k^c$ does not describe the real channel between the AP and *SenCom*. If the sniffed packets are from the client that *SenCom* is implemented on, the obtained $\boldsymbol{H}_k^c$ can be directly used for sensing and there is no need to listen to the feedback of NDP. Without loss of generality, for the cases where the sniffed packets are from the clients without implementing *SenCom*, $\boldsymbol{V}_{k,N_{STS}}$ can be derived from $\boldsymbol{H}_k^c$ suppose that we know the structuring method of the adopted beamforming scheme. Here, we assume that the AP adopts zero-forcing (ZF) beamforming [33], as it is one of the most popular ones [34]. Then, after sniffing the CSI measured by the client (i.e., $\boldsymbol{H}_k^c$), the steering matrix can be calculated at *SenCom* by: $\boldsymbol{V}_{k,N_{STS}} = ((\boldsymbol{H}_k^c)^H\boldsymbol{H}_k^c)^{-1}(\boldsymbol{H}_k^c)^H$, where $(\cdot)^H$ represents the operation of conjugate transpose. Under the premise that *SenCom* has the knowledge of the beamforming strategy employed by the AP, the above compensation method can be easily extended to other beamforming schemes by simply replacing the steering matrix. For example, for the singular value decomposition (SVD) beamforming [28], the steering matrix can be given by $\boldsymbol{V}_k$ with the SVD of the CSI measured by the client (i.e., $\boldsymbol{H}_k^c$) being $\boldsymbol{H}_k^c = \boldsymbol{U}_k\boldsymbol{\Sigma}_k\boldsymbol{V}_k$. This approach provides *SenCom* with a mechanism to estimate the steering matrix even when the feedback comes in the form of uncompressed beamforming feedback.

Under compressed beamforming feedback, the client first performs SVD as $\boldsymbol{H}_k^c = \boldsymbol{U}_k\boldsymbol{\Sigma}_k\boldsymbol{V}_k$ after measuring the CSI, and then feeds $\boldsymbol{V}_k$ back to the AP. The AP directly utilizes $\boldsymbol{V}_k$ as the steering matrix $\boldsymbol{V}_{k,N_{STS}}$ to achieve beamforming, which means $\boldsymbol{V}_{k,N_{STS}} = \boldsymbol{V}_k$. Therefore, the sniffed feedback can be directly used to recover $\boldsymbol{V}_{k,N_{STS}}$.

After obtaining $\boldsymbol{V}_{k,N_{STS}}$ under two feedback types, *SenCom* can effectively suppress the impact of beamforming with the compensation formula (Eq. 12).

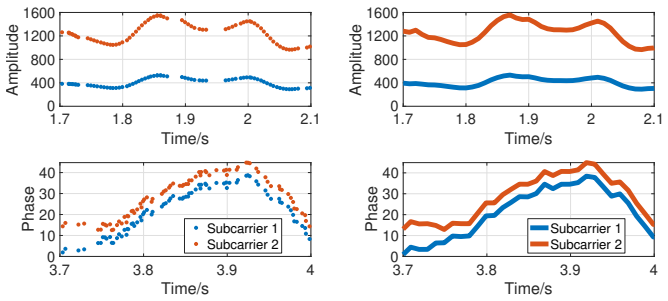

(a) CSI amplitude/phase variation traces of two subcarriers. (b) Fitted CSI amplitude/phase curves of two subcarriers.

Fig. 5. Cubic spline fitting results.

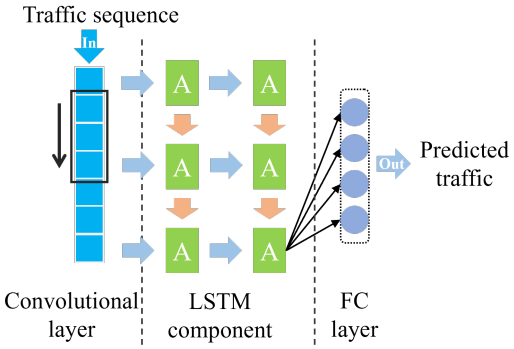

Fig. 6. Neural network-based traffic predictor.

V. Unifying CSI Sampling

In traditional WiFi sensing, packets are transmitted consistently at evenly-spaced intervals. This practice ensures a consistent dimensionality of sampled CSI, which is crucial for upper-layer sensing applications. However, maintaining such uniformity is challenging due to variable downlink data demands in communication traffic. To address this issue, we devise a fitting-resampling scheme aimed at preserving the uniformity of CSI scatters in the time domain. In cases the normal communication packets are insufficient, we propose an incentive strategy to encourage the AP to send compensation packets. In its design, we model the trade-off between the sensing and communication performance, ensuring that *SenCom* can acquire adequate packets without causing a significant degradation in the communication.

A. Fitting and Resampling

When clients require high communication demands, *SenCom* can successfully acquire sufficient packets for sensing. Nevertheless, the distribution of communication packets over time is not uniform, leading to variability in the number of packets collected within a fixed-length time interval. This fluctuation poses a challenge in ensuring that the input CSI samples maintain consistent dimensionality, a critical requirement for many sensing systems' upper-layer applications, especially those employing learning models. For instance, consider the WiFi-based sign language recognition system, SignFi [35], which utilizes CSI amplitude with a default fixed dimensionality of (3, 30, 200). Here, the 3×30 dimension corresponds to the number of subcarriers, and the last dimension represents the collection of 200 packets evenly for each CSI sample. To address this issue, we propose to fit the variation trace of each subcarrier in the CSI sample, and subsequently resample the fitted function at an equal interval. Specifically, we opt to perform cubic spline fitting, because we observed that the variation trace of each subcarrier is akin to the splicing of multiple cubic functions in the time domain (i.e., cubic function in each small time window). The fitting results of two subcarriers are shown in Fig. 5. It can be observed that the fitted curves (Fig. 5(b)) closely resemble the real variation traces of the subcarriers (Fig. 5(a)). Therefore, cubic spline curves can precisely fit the sensing information recorded by CSI. Subsequently, we sample these spline functions at uniform intervals, allowing *SenCom* to maintain a consistent sampling rate and provide dimensionality-consistent CSI samples for upper-layer applications.

B. Incentive Strategy

In scenarios where clients exhibit no communication demands, there is no ongoing packet for *SenCom* to sample the CSI. To tackle this issue, we develop an incentive strategy based on queuing theory [36]. This strategy enables *SenCom* to transition between two states in order to acquire sufficient incentive packets (i.e., probing packets) while minimizing any substantial impact on communication performance.

State definition. We assume that the arrival process of communication packets at the AP follows the Poisson process [37] with a rate $\lambda^c[t]$ (in packets/s) at time index t. Let F^{re} (in packets/s) be the required sensing frequency, i.e., the required CSI sampling rate. By comparing F^{re} with $\lambda^c[t]$, we have the following two states within the incentive strategy. (i) *Silent state*: it refers to the state when $\lambda^c[t] \geq F^{re}$. In this state, the AP does not need to transmit incentive packets and *SenCom* solely measures CSI from communication packets. (ii) *Incentive state*: it refers to the state when $\lambda^c[t] < F^{re}$. In this state, *SenCom* encourages the AP to transmit incentive packets with an incentive rate $\lambda^i[t]$ by 'pinging' the AP and collects CSI simultaneously.

Traffic prediction. To conduct state transition at the most appropriate time point, we can opt to predict the upcoming network traffic based on historical traffic information [38]. Specifically, we can use supervised learning technique to train a neural network-based traffic predictor. As shown in Fig. 6, the predictor is composed of a convolutional layer, a long short-term memory (LSTM) component, and a fully-connected (FC) layer. The convolutional layer performs one-dimensional convolution along the historical traffic sequence to extract local temporal features. The LSTM component has two hidden layers. It can capture the long-term dependence in the sequence to further improve the prediction ability. The FC layer is responsible for mapping the extracted features to future traffic information. An input traffic sequence can be denoted as: $\{x_{t_1}, x_{t_2}, x_{t_i}, \cdots, x_{t_m}\}$. x_{t_i} is the number of packets transmitted within $[t_{i-1}, t_i]$ and is given by $x_{t_i} = \lambda^c[t_i](t_i - t_{i-1})$. Each traffic sequence is annotated/labeled by the so-called future packet number, i.e., the number of packets transmitted within $[t_m, t_{m+1}]$. After training, the neural network is able

to predict the unknown upcoming traffic information (i.e., $x_{t_{m+1}}$) based on the real previous traffic measurements. The parameters in the predictor can be optimized by minimizing the root mean-square logarithmic error (RMSLE) [39]:

$$RMSLE = \sqrt{\frac{1}{n}\sum_{i=1}^{n}(\log(y_i{}' + 1) - (\log(y_i + 1))^2}, \quad (13)$$

where n is the number of training traffic sequences, $y_i{}'$ is the predicted packet number, and y_i is the ground truth. We can use Adam optimizer to update parameters. To collect training data, users can implement *SenCom* in the target environment for a period of time to monitor the traffic at first. Empirically, 8600 pieces of data are sufficient for traffic predictor training [38]. To make the traffic predictor adapt to a new environment without introducing huge data collection overhead, *SenCom* can optimize it with a small training set collected in the new environment with transfer learning [40], where only the last fully-connected layer needs to be fine-tuned.

Incorporating communication loss. Moving forward, our primary concern lies in evaluating the performance during the incentive state, as transmitting incentive packets can potentially impact communication performance. We aim to ensure that ongoing communication traffic remains unaffected when we inject additional probing packets in the incentive state. As demonstrated by prior studies [14], [41], [42], the sensing performance is positively related to the CSI sampling rate since a higher sampling rate provides more information about the sensing target, thereby improving the sensing performance. Meanwhile, CSI is measured from the packets transmitted by the WiFi AP, and there are two types of packets, i.e., the communication packet with the arrival rate being $\lambda_c[t]$ and the incentive packets with the arrival rate being $\lambda_i[t]$. Thus, the total number of packets transmitted by the AP per unit time is $\lambda_i[t] + \lambda_c[t]$, and the number of CSI samples measured from these packets per unit time (i.e., CSI sampling rate) at the *SenCom* is also $\lambda_i[t] + \lambda_c[t]$. Consequently, the sensing performance can be represented by $\lambda_c[t] + \lambda_i[t]$. Meanwhile, the communication performance can be analyzed using queueing theory. As we assume that the arrival of packets is **M**arkovian (modeled as a Poisson process), the transmission latency (i.e., service time) has a **G**eneral distribution, the packet queue at **one** Wi-Fi AP can be regarded as a M/G/1 queue [36]. The communication latency without incentive packets is given by:

$$\tau^c[t] = \frac{\lambda^c[t]\mathbb{E}\left\{W^2\right\}}{2\left(1 - \lambda^c[t]\mathbb{E}\left\{W\right\}\right)} + \mathbb{E}\left\{W\right\}. \quad (14)$$

Here, W represents the transmission latency and $\mathbb{E}\left\{\cdot\right\}$ denotes the expectation operation. With $\lambda^c[t]\mathbb{E}\left\{W\right\} < 1$, every packet is successfully delivered, and the corresponding throughput is the product of the rate $\lambda^c[t]$ and the data size per packet. In contrast, when incentive packets are introduced, the communication latency becomes:

$$\tau^{c,i}[t] = \frac{\left(\lambda^c[t] + \lambda^i[t]\right)\mathbb{E}\left\{W^2\right\}}{2\left(1 - \left(\lambda^c[t] + \lambda^i[t]\right)\mathbb{E}\left\{W\right\}\right)} + \mathbb{E}\left\{W\right\}. \quad (15)$$

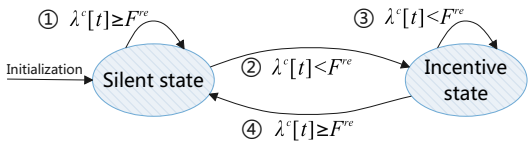

Fig. 7. Incentive strategy.

Furthermore, when $\left(\lambda^c[t] + \lambda^i[t]\right)\mathbb{E}\left\{W\right\} < 1$, the throughput remains unchanged. Therefore, our primary focus lies on the *latency loss*, as $\Delta\tau[t] = \tau^{c,i}[t] - \tau^c[t]$.

Balancing sensing and communication. To enable efficient sensing without compromising communication, we formulate the following optimization problem:

$$\max_{\lambda^i[t]} \quad \beta\left(\lambda^c[t] + \lambda^i[t]\right) - (1-\beta)\Delta\tau[t], \quad (16a)$$

$$\text{s.t.} \quad \left(\lambda^c[t] + \lambda^i[t]\right)\mathbb{E}\left\{W\right\} \leq 1 - \epsilon, \quad (16b)$$

$$\lambda^i[t] \geq 0, \quad (16c)$$

where β denotes the weight and $\epsilon > 0$ denotes the tolerance. The objective function in Eq. 16a describes the trade-off between sensing performance and communication latency. The constraint in Eq. 16b ensures that the communication throughput remains unaffected by the presence of incentive packets. It is easy to prove the convexity of the above problem and the corresponding optimal solution is given by:

$$\lambda^{i,\star}[t] = \left[\frac{1}{\mathbb{E}\left\{W\right\}}\left(1 - \sqrt{\frac{1-\beta}{2\beta}\mathbb{E}\left\{W^2\right\}}\right) - \lambda^c[t]\right]_0^{\frac{1-\epsilon}{\mathbb{E}\{W\} - \lambda^c[t]}}, \quad (17)$$

where $[x]_A^B = \min\{B, \max\{x, A\}\}$. The additional details can be found in Appendix A. From Eq. 17, it is evident that the incentive rate $\lambda^i[t]$ is influenced by β. If we prefer better sensing performance than less communication loss, we can empirically set a high β to get a large incentive rate.

Overall view. The optimal incentive rate in the incentive state is now clear. As shown in Fig. 7, the incentive strategy contains two states, and the transition conditions between the two states are determined by the arrival rate of communication packets $\lambda^c[t]$ and the required sensing frequency F^{re}. If $\lambda^c[t] \geq F^{re}$, the subsequent state is the silent state; otherwise, the next state is the incentive state. In the silent state, *SenCom* acquires CSI by passively monitoring communication packets and driving the AP to transmit incentive packets with rate $\lambda^i[t]$ given in Eq. 17. This design effectively addresses the issue of CSI insufficiency while keeping communication loss very low.

VI. Evaluation

This section presents the real-world implementation and details the performance of *SenCom* in terms of sensing and communication.

A. Implementation

As shown in Fig. 8, we implement *SenCom* on a standalone sensing client comprising a CSI monitor, a packet monitor, and an intelligent unit. Not using an off-the-shelf client to embark *SenCom* is indeed an engineering compromise. Even though most existing WiFi network interface cards (NICs)

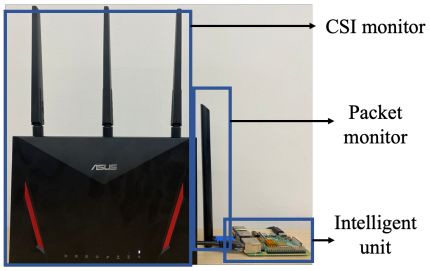

Fig. 8. Prototype of *SenCom*.

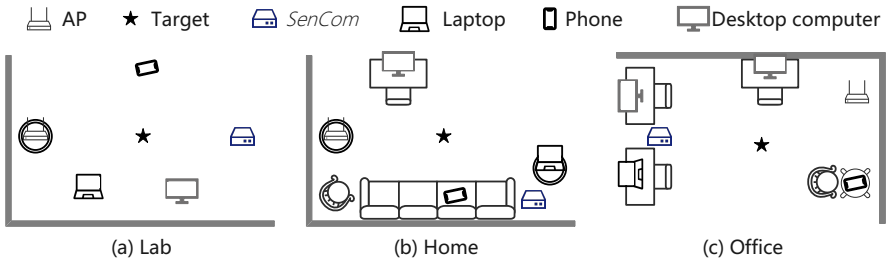

Fig. 9. Three environments for *SenCom* evaluation.

on the clients are able to sniff packets and measure the CSI, the NIC manufacturers do not provide corresponding permissions as these abilities are useless for upper-layer non-sensing applications. Nonetheless, it is noteworthy that NICs are technically capable of performing all the functions required by *SenCom*, and it is technically trivial to modify *SenCom* to work with a single WiFi NIC should the CSI information is internally accessible from the NIC. We believe that our work will encourage manufacturers to open the interfaces for these abilities. In *SenCom* prototype, the CSI monitor measures CSI from received packets, while the packet monitor is responsible for receiving the feedback of beamforming. The intelligent unit wirelessly connects to an AP and performs incentive strategy, CSI calibration, fitting, resampling, and finally gets the sensing result. More specifically, we implement *SenCom* on a Raspberry Pi 4B connected to a TP-LINK WDN5200H (a Wireless USB WiFi Adapter) and an ASUS RT-AC86U Router. The Raspberry Pi 4B works as the intelligent unit, and the TP-LINK WDN5200H is configured in the monitor mode working as the packet monitor. The ASUS RT-AC86U Router installed with the Nexmon CSI tool [43] is used as the CSI monitor. Note that we have modified Nexmon CSI tool so that it can distinguish whether beamforming is utilized in the packet while logging CSI from the received packet.

We conduct experiments in three different environments (a lab, a home, and an office) as shown in Fig. 9. To mimic a real communication scenario, a Mi Router Mini and three clients are included. The router works as an AP with a bandwidth of 20 MHz. The clients include a laptop with a one-antenna wireless adapter (TP-LINK WDN5200H), a phone (Google Pixel 4) with two antennas, and a desktop computer with a three-antenna network interface card (TP-LINK TL-WDN7280). In default communication context, the Google Pixel 4 phone is connected to the AP and plays online videos. Moreover, to show the performance of *SenCom*, we adopt a baseline, i.e., traditional Active sensing systems. In the experiments of Active sensing, we also use the WiFi AP as the transmitter and the client equipped with *SenCom* as the receiver but there is no other client. The WiFi AP transmits packets to the client without beamforming and communication mode alternation under a fixed sensing packet rate, so that there is no influence on sensing performance from communication settings.

We focus on the standard of 802.11ac Wave 1 since it is one of the most pervasive WiFi standards in existing WiFi devices. In this standard, OFDM, MIMO, packet aggregation, beamforming, and other techniques are adopted to enhance channel efficiency. Our work can also be easily extended to the subsequent WiFi standards (i.e., 802.11ac Wave 2 and 802.11ax) and 4G/5G standard, where orthogonal frequency division multiple access (OFDMA) and multi-user multiple-input multiple-output (MU-MIMO) are adopted for high communication performance. With the OFDMA, the AP can allocate different subcarriers to different users for simultaneous transmission. OFDMA does not affect sensing performance as it does not influence the collected CSI at *SenCom*. As for the MU-MIMO, it is an extended version of the beamforming mentioned above and the steering matrix is constructed for multi-user simultaneous transmission by sniffing the feedback of NDP. Therefore, the proposed CSI calibration method for beamforming can be easily extended to deal with the impact brought by MU-MIMO as well. Besides, it is well known that WiFi signals are environment-dependent. The sensing model trained over the data collected in one environment may perform inadequately in another. Fortunately, previous studies [5], [44] have proposed lots of solutions that can be directly integrated into the upper-layer applications of *SenCom*. Taking environment-independent activity recognition as an example, users can first collect WiFi signals from multiple environments via *SenCom*. Then, an adversarial neural network can be trained over these signals to extract environment-independent activity features. Any classifier trained with such features will possess the ability of cross-environment activity recognition [5]. In addition, users can also directly extract Doppler frequency shift (DFS) from the WiFi signals collected by *SenCom*. As DFS is only activity-specific, it can be leveraged to train an environment-independent activity recognition model [44].

B. Sensing Performance

In this part, we measure the sensing performance of *SenCom*. We conduct two types of experiments to verify the effectiveness of the CSI calibration and incentive strategy, respectively. These experiments inspect both the quality and quantity of the CSI collected at *SenCom*.

1) Experiment Setup and Metric: **Experiment setup:** To test the performance of the CSI calibration, we collect the CSI samples during the coherence time and compare the calibrated CSI of $N_{STS} \geq 2$ with the collected CSI of $N_{STS} = 1$. To test the performance of the incentive strategy, we expose *SenCom* to the real WiFi communication environment and perform the incentive strategy. We adopt two baseline schemes for comparison: traditional WiFi sensing (Active), and passive CSI collection without calibration and incentive (Passive). In theory, Active sensing can achieve the best sensing performance. Over 20,000 CSI samples are collected during the experimental evaluation.

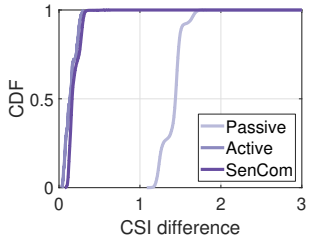

Fig. 10. CDF of CSI difference.

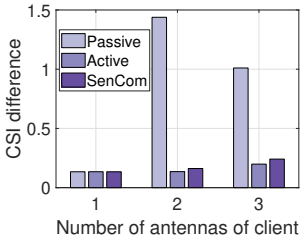

Fig. 11. Median of CSI differences with different client's antenna numbers.

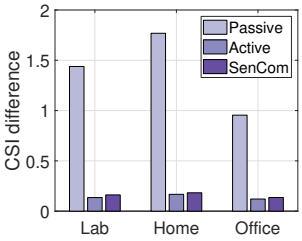

Fig. 12. Median of CSI differences in three environments.

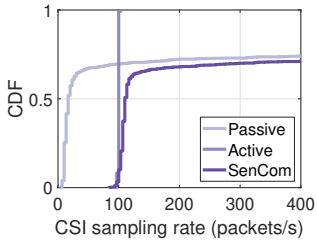

Fig. 13. CDF of CSI sampling rate.

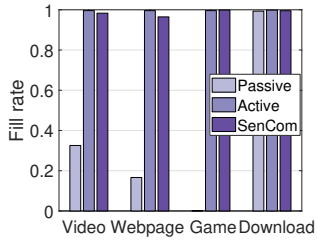

Fig. 14. Fill rates with different communication tasks.

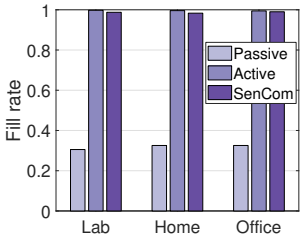

Fig. 15. Fill rates in three environments.

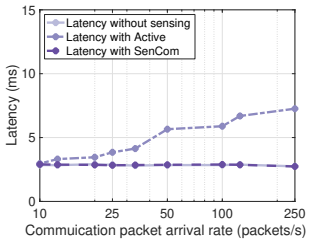

Fig. 16. Communication latency.

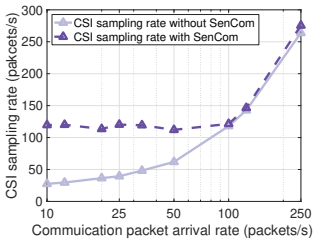

Fig. 17. CSI sampling rate.

Metrics: For the CSI calibration, we adopt *dynamic time warping (DTW)* [45] to measure the *CSI difference* between the calibrated CSI of $N_{STS} \geq 2$ and the collected CSI of $N_{STS} = 1$. It seeks the temporal alignment that minimizes Euclidean distance between aligned series and the CSI difference is defined as the minimal Euclidean distance. A lower CSI difference indicates lower deviations between the measured CSI from different modes, i.e., better performance of CSI calibration. All CSI samples are normalized to eliminate the effect of variation of channel gain. For the incentive strategy, we adopt *fill rate* to quantify its performance, which is defined as the probability of meeting the required CSI sampling rate. It is calculated as the ratio of the number of tests that meet the such requirement to the number of all tests. The time window of each test is set to 0.3 s. Although the expected CSI sampling rate is 100 packets/s, the sensing requirement is set as 95 packets/s since there would be a loss of packets even in active sensing.

2) Results: **Effectiveness of CSI calibration:** The cumulative distribution function (CDF) of the CSI difference for the three schemes is shown in Fig. 10. It can be seen that the CSI difference of Passive sensing is much higher than that of Active sensing, which indicates the low CSI quality issue due to the alternation of WiFi communication modes. By using the proposed CSI calibration method, the CSI difference of *SenCom* is greatly reduced to the level of Active sensing, without the need for active communication or coordination with the AP. Further, we show the median of the CSI difference with different client's antenna numbers in Fig. 11. The CSI difference of *SenCom* reaches that of Active sensing, which demonstrates that the CSI calibration can improve the quality of CSI. Besides, the CSI differences of the three schemes are almost the same when the antenna number is 1 because all packets are in the same communication mode. We also show the median of the CSI difference in three environments in Fig. 12. It can be found that the performance of the CSI calibration is not affected by the environment.

Effectiveness of incentive strategy: The CDF of CSI sampling rate is shown in Fig. 13. It can be found that the CSI sampling rate of Active sensing is stable, that is, about 100 packets/s all the time. On the contrary, when the client is playing an online video, the probability that the CSI sampling rate is higher than 100 packets/s is around 30% and the CSI sampling rate is less than 40 packets/s in most cases, which cannot satisfy the sensing requirement at all times and may lead to the missing of key sensing information. It can be observed that the CSI sampling rate tends to exceed 100 packets/s with our proposed incentive strategy. In practical daily life, however, people may perform a variety of tasks on the Internet, such as visiting websites and playing online games. The fill rate for four communication tasks (namely video streaming, webpage surfing, online gaming, and download) are shown in Fig. 14. *SenCom* gives almost the same performance as that of Active sensing under different communication tasks, which demonstrates its effectiveness. The fill rate approaches 100% for the task of download as its communication demands are frequent and stable. Meanwhile, the medians of CSI sampling rate for the four communication tasks are 20.0 packets/s, 13.3 packets/s, 30.0 packets/s, and 503.3 packets/s, respectively. The corresponding intervals are 50.0 ms, 75.0 ms, 33.3 ms, and 2.0 ms, respectively. After applying the incentive strategy, the medians of CSI sampling rate for the four communication tasks are all higher than the sensing requirement. In addition, we also test the incentive strategy in three environments, as shown in Fig. 15. It can be seen that the fill rates are similar and near 100%. This indicates that the sensing requirement for sufficient CSI can be satisfied in different environments with our incentive strategy.

3) Time Consumption: To assess the real-time performance of *SenCom*, we calculate the time spent on CSI calibration and fitting-resampling. The experiment results indicate that *SenCom* can unify a CSI sample in 0.86 ms and homogenize

TABLE II
COMMUNICATION PERFORMANCE WITH DIFFERENT COMMUNICATION TASKS.

Task	Video	Webpage	Game		Download
Metric	Dropped rate	Loading time	Latency	Loss rate	Data rate
Without *SenCom*	1597/40477	614 ms	17 ms	0 %	88.68 Mbps
With *SenCom*	1613/40477	615 ms	17 ms	0 %	87.12 Mbps

TABLE III
COMMUNICATION LATENCY WITH DIFFERENT ERRORS OF TRAFFIC PREDICTION.

Error (packets per 100 ms)	0	1	2	3
Latency (ms)	2.84	2.94	3.03	3.14

the sampling points in 1.76 ms. The entire time consumption is only 2.62 ms, less than the required interval of the CSI sample, i.e., 10 ms. Thus, *SenCom* can provide quality and sufficient CSI to upper-layer applications in real time.

C. Communication Performance

In this part, we measure the impact of *SenCom* on the normal WiFi communication performance.

1) Experiment Setup and Metric: **Experiment setup:** We test the communication performance in two ways. One is to directly measure the communication performance with the help of iperf between the AP and client. The other is to measure the quality of experience (QoE) of the four aforementioned communication tasks. The communication performance is tested in a week randomly and the total time is more than 10 hours. Average results are shown in this part.

Metrics: For the direct measurement, we adopt two metrics, i.e., *latency* and *throughput*, to quantify the communication performance. Latency describes the end-to-end delay between the AP and the client. Throughput is measured by the rate of successfully delivered data between the client and AP, which can be calculated as throughput $= \eta\lambda^c V$, where η is the successful delivery rate, λ^c is the packet arrival rate, and V is the data size per packet. For the task of webpage surfing, we utilize the *loading time* of the website to measure the QoE. For video streaming, its QoE is represented by the fluency of the video, i.e., *dropped rate* that is the number of dropped frames to the total number of frames. As for online gaming, we can use *latency* between the client and the game server and *loss rate* of operations. For the download task, its QoE is described by the data size delivered successfully per unit time, i.e., *data rate*.

2) Results: We evaluate the latency and throughput with different communication packet arrival rates. As shown in Fig. 16, the communication latency with *SenCom* is almost the same as that without *SenCom*. Especially, when the communication packet arrival rate is no less than the required CSI sampling rate, i.e., $\lambda^c \geq 100$ packets/s, there is no need to transmit incentive packets, and the latency thus is not affected at all. When $\lambda^c < 100$ packets/s, the loss can be reduced to a negligible level, i.e., less than 2%, by choosing a proper weight (i.e., $\beta = 0.1$). Moreover, we evaluate the latency when Active sensing and the communication systems simultaneously work on the same frequency bandwidth. One can clearly observe that the latency is higher than that without sensing, demonstrating the influence of active sensing on communication. Meanwhile, according to the experiment results, the successful delivery rate without *SenCom* and with *SenCom* is 100%, indicating that *SenCom* does not affect the throughput. Moreover, Fig. 17 shows the average CSI sampling rate. With the incentive strategy, the CSI sampling rate is maintained constantly higher than required. By contrast, without the incentive strategy, the CSI sampling rate may fall short when the communication packet rate is low. Additionally, we also evaluate the effect of the traffic prediction error on the communication latency when the communication packet arrival rate is 50 packets/s. As shown in Tab. III, the error is represented by the difference between the real packet number and predicted one per 100 ms and we focus on the case that the predicted number is larger than the actual one since the communication latency would be increased in this case. From Tab. III, it can be seen that the impact of the error on delay is small, as the communication traffic is not congested and few extra incentive packets would not bring significant impact. When the communication traffic is congested, i.e., the number being more than 100 packets/s, the error would not affect the latency because there is no need to transmit incentive packets.

The QoE of the four communication tasks is shown in Tab. II. It can be observed that *SenCom* almost has no influence on the QoE of the communication tasks. Even for the download task that requires a very high data rate, the communication traffic is hardly impacted by the incentive strategy. Recalling that the required CSI sampling rate can be guaranteed according to the results in Fig. 14. Hence, with *SenCom* implemented in the communication system, sufficient CSI can be obtained for sensing without influencing ongoing communication traffic too much.

D. Case Study

We invite 22 volunteers (13 males and 9 females) aged from 19 to 29 to take part in the following four WiFi sensing applications: fall detection (WiFall [46]), step counting (WiStep [21]), respiration monitoring (WiBreath [47]), and person identification (WiPIN [24]). WiFall and WiPIN are classification applications, while WiStep and WiBreath are measurement applications. The required CSI sampling rate is set to 100 packets/s. We collect over 35,000 CSI samples for case studies. All experiments are conducted by adhering to the approval of our university's Institutional Review Board.

1) Fall Detection: WiFall is a learning-based fall detection system, which utilizes a random forest classifier to recognize four activities including 'walking', 'sitting down', 'standing up', and 'falling'. We use *accuracy* [46] to quantify the classification performance.

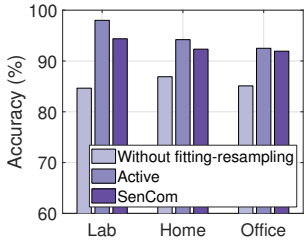

Fig. 18. Accuracy of fall detection in three environments.

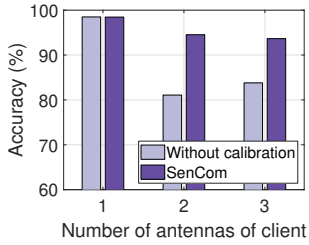

Fig. 19. Effect of client's antenna number on accuracy of fall detection.

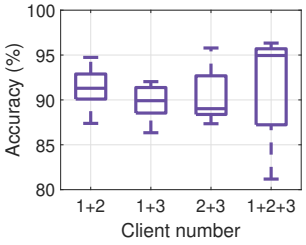

Fig. 20. Effect of client number on accuracy of fall detection.

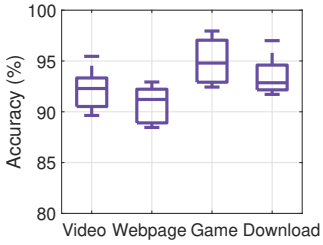

Fig. 21. Effect of client activity on accuracy of fall detection.

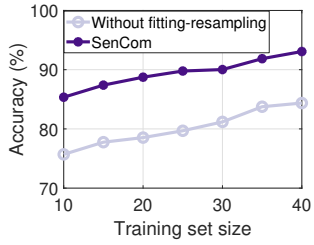

Fig. 22. Effect of training set size on accuracy of fall detection.

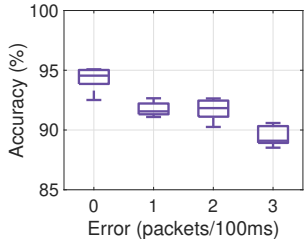

Fig. 23. Effect of traffic prediction's error on accuracy of fall detection.

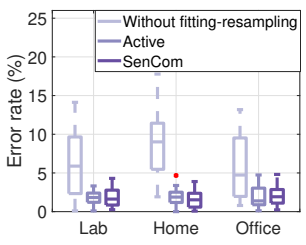

Fig. 24. Error rates of step counting in three environments.

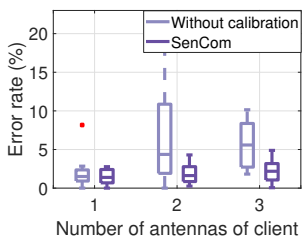

Fig. 25. Effect of client's antenna number on error rate of step counting.

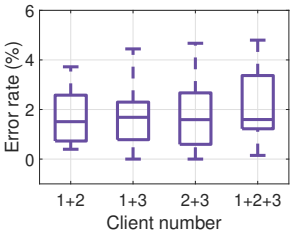

Fig. 26. Effect of client number on error rate of step counting.

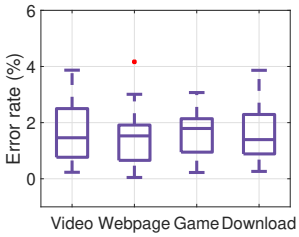

Fig. 27. Effect of client activity on error rate of step counting.

Overall performance. We first derive the activity recognition accuracy when supporting WiFall in three environments. We compare *SenCom* with two schemes: simply collecting CSI without fitting-resampling, and Active sensing. The average accuracy of five persons in each environment is recorded. The accuracy of the three environments is shown in Fig. 18. It can be found that the accuracy of *SenCom* is higher than that without fitting-resampling. Thus, our fitting-resampling method can improve the activity recognition accuracy. The accuracy of *SenCom* is comparable to that of Active sensing, indicating that *SenCom* is qualified for classification tasks. Meanwhile, the accuracy of *SenCom* in lab, home, and office is 94.37%, 92.33%, and 91.93%, respectively. The accuracy is high and similar, demonstrating that *SenCom* performs well in different environments. The small accuracy differences are likely to be induced by random environmental noise. The results suggest that *SenCom* can achieve outstanding performance in classification tasks.

Effect of client's antenna number: In this part, we use three clients equipped with one, two, and three antennas to explore the effect of the client's antenna number. To show the effectiveness of our CSI calibration method, we compare *SenCom* with an alternative: without CSI calibration. The experimental results of activity recognition are shown in Fig. 19. It can be seen that the performance when using one antenna is better than that of using two or three antennas. This is reasonable because *SenCom* does not need to execute CSI calibration when the client has only one receiving antenna. The CSI collected in this case is of higher quality. Meanwhile, the performance of *SenCom* is better than that of the alternative, which means that our CSI calibration method is very effective in improving the quality of CSI.

Effect of client number: In practice, multiple client devices may co-exist in the same WiFi domain. In this case, the transmitter is connected with multiple clients and transmits packets to different clients across time. To explore the effect of the client number, we conduct four experiments with four conditions. The experimental results of activity recognition are displayed in Fig. 20, where '$1+2$' means that the transmitter is connected with a one-antenna client and a two-antenna client, and so forth. It can be observed that the performance of *SenCom* with different conditions is good and very similar to each other. This demonstrates the effectiveness of the CSI calibration, and as a result, the varied number of clients hardly affects the classification performance.

Effect of client activity: We also consider other communication traffic, i.e., online video, online gaming, webpage surfing, and download. Fig. 21 depicts the activity recognition results when *SenCom* works with the above different communication traffic. As during download, the client has high communication demands, we disable the signal incentive. In Fig. 21, it can be found that online gaming can achieve the highest average accuracy. The number of communication packets under the online gaming task is few and even approaches zero as indicated by Fig. 14 and most CSI is extracted from incentive packets that do not need to be calibrated, rendering better performance. But it is noteworthy that *SenCom* still performs well (93.53% accuracy) under the worst conditions (i.e., download) where all the packets are from the communication traffic. This further demonstrates the effectiveness of our CSI calibration method.

Effect of training set size: Since WiFall adopts a learning-based method to achieve activity recognition, the size (i.e.,

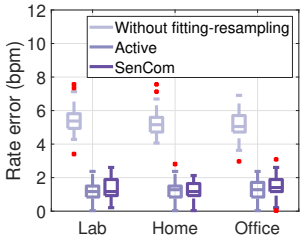

Fig. 28. Rate errors of respiration monitoring in three environments.

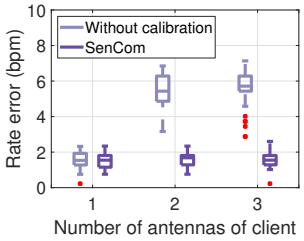

Fig. 29. Effect of antenna number on rate error of respiration monitoring.

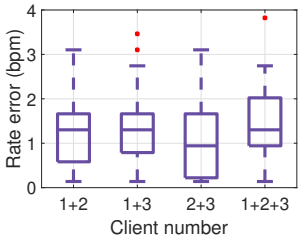

Fig. 30. Effect of client number on rate error of respiration monitoring.

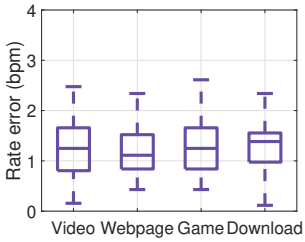

Fig. 31. Effect of client activity on rate error of respiration monitoring.

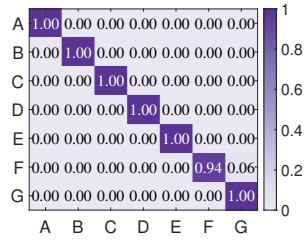

Fig. 32. Identification performance of Active sensing.

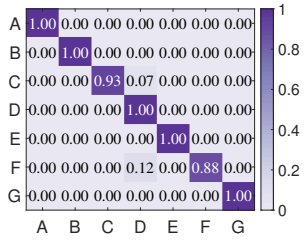

Fig. 33. Identification performance of *SenCom*.

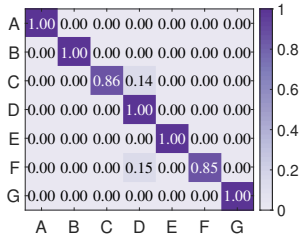

Fig. 34. Identification performance without fitting-resampling.

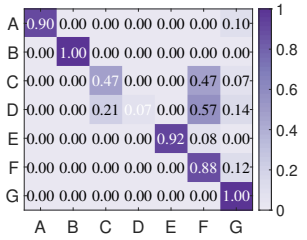

Fig. 35. Identification performance without CSI calibration.

the number of CSI samples) of the training set directly affects the activity recognition result. To explore if *SenCom* can still work well when the training set is small, we vary the number of the training CSI samples of each class from 10 to 40 and calculate the accuracy. Meanwhile, we compare *SenCom* with an alternative: without fitting-resampling. It can be observed from Fig. 22 that *SenCom* outperforms the alternative and the accuracy of two schemes increases with the number of the training CSI samples. When the number of CSI samples of each activity is 40, the accuracy reaches the highest. Nevertheless, the accuracy is still high (85%+) when only 10 CSI samples are collected for each class, which indicates that *SenCom* is insensitive to the training data size.

Effect of traffic prediction's error: We propose a traffic predictor to predict the upcoming network traffic for incentive strategy and the error of the traffic predictor may affect the CSI sampling rate and sensing performance. Fig. 23 presents the effect of traffic prediction error on accuracy. The error is represented by the difference between the real packet number and predicted one per 100 ms and we consider the case that the predicted number is smaller than the actual one as the deficiency of packets would reduce the sensing performance. One can observe that the accuracy reduces with the error and the average accuracy is still around 90% when the prediction error is 3 packets per 100 ms (70% prediction accuracy). This means that the prediction error indeed impacts the sensing performance, yet *SenCom* is robust to the prediction deviation thanks to our fitting-resampling method.

2) Step Counting: WiStep is a modeling-based step counting system that can measure the number of steps with CSI samples. We use *error rate* [21] to qualify the measurement performance, which is the relative error between the estimated step count R_e and the ground truth value R_g, i.e., $error\ rate = |R_e - R_g|/R_g$.

Overall performance. For step counting, we conduct comparison experiments similar to the activity recognition. The experimental results shown in Fig. 24 indicate that *SenCom*'s average error rates in lab, home, and office are 1.8%, 1.6%, and 2.0%, respectively. Meanwhile, it can be observed that our fitting-resampling method is also effective in measurement tasks. More importantly, the error rate of *SenCom* is comparable to that of Active sensing. The results prove that *SenCom* can effectively support measurement tasks.

Effect of client's antenna number: This experiment investigates the effect of antenna number of the communication client. Similar to the experiment setting of activity recognition, we also compare *SenCom* with an alternative, i.e., directly sensing without CSI calibration. Fig. 25 shows the measurement results. We can see that *senCom* can achieve the best performance when the client only has one antenna. Such a conclusion is consistent with that drawn from the activity recognition experiment. Moreover, *SenCom* outperforms the alternative, demonstrating the efficacy of the CSI calibration.

Effect of client number: To understand the effect of client number on measurement, we perform experiments with different client combinations. The results in Fig. 26 suggest that *SenCom* can accurately measure the step with different client numbers, demonstrating the effectiveness of the proposed methods.

Effect of client activity: We also explore the effect of client activity on measurement performance. The experiment results are shown in Fig. 27. It can be seen that *SenCom* demonstrates a very low error rate (less than 1.65%) under all activities.

3) Respiration Monitoring: WiBreath utilizes short-time Fourier transform (STFT) to get the respiration frequency of the monitored user from CSI. We use *rate error* to quantify the performance, which is defined as the difference between the estimated respiration rate R_e and the ground truth value R_g, i.e., $rate\ error = |R_e - R_g|$.

Overall performance: Fig. 28 shows the rate errors of respiration monitoring in the three environments. It can be seen that the rate error of *SenCom* is comparable to that of Active sensing. Meanwhile, the rate error will increase obviously if the fitting-resampling is not adopted. Besides, the environment

changes do not significantly impact the respiration monitoring performance.

Effect of client's antenna number: To understand how the respiration monitoring rate error would be impacted by the number of the client's antennas, we experiment over three clients with different antennas. As shown in Fig. 29, the rate error seems to not vary evidently with the number of antennas. *SenCom* can monitor user's respiration accurately under different clients. Meanwhile, it can be found that calibrating the CSI can greatly improve the respiration monitoring precision.

Effect of client number: In this experiment, we assess *SenCom*'s performance under different numbers of clients. The results in Fig. 30 indicate that *SenCom* performs fairly in different settings. Even over three clients equipped with different antenna numbers, *SenCom* still demonstrates low rate error. Thus, *SenCom* can adapt to different client combinations.

Effect of client activity: We also evaluate the rate error when the client runs different applications. One can observe from Fig. 31 that the applications like playing video hardly affect the respiration monitoring performance of *SenCom*. Downloading will trigger a large number of communication packets, but this does not reduce the rate error. Hence, our CSI calibration method is very effective.

4) Person Identification: WiPIN collects CSI when the user is standing still between the transmitter and receiver. It extracts several statistical features as biometrics and uses the support vector machine (SVM) to identify users. Its performance is also qualified by *accuracy*. In this experiment, WiPIN needs to identify seven persons, including three males and four females.

Overall performance: To illustrate the person identification performance, we plot the confusion matrices of Active sensing and *SenCom* in Figs. 32 and 33, respectively. 'A' to 'G' represent seven different persons. It can be seen that the accuracy of Active sensing and *SenCom* is 98.80% and 97.62% respectively. Active sensing slightly outperforms *SenCom*, but the accuracy difference is very small. Thus, *SenCom* demonstrates outstanding person identification performance.

Effectiveness of fitting-resampling: To validate that fitting-resampling can improve the person identification accuracy, we recalculate the confusion matrix when the fitting-resampling method is not used. The results in Fig. 34 indicate that the accuracy is only 95.24%, suggesting that our fitting-resampling measure is effective in enhancing the sensing performance.

Effectiveness of CSI calibration: We also assess the identification accuracy when the CSI is not calibrated. The corresponding confusion matrix is shown in Fig. 35. It can be observed that the accuracy drops to 71.4% when we do not perform calibration. This means that our calibration approach can greatly improve the CSI quality to support accurate sensing.

VII. Conclusion

In this paper, we propose *SenCom*, which enables WiFi sensing while maintaining communication capabilities. *SenCom* reuses the communication facilities and packets for sensing. In its design, we propose a CSI calibration method to obtain quality and unified CSI. Additionally, we introduce a fitting-resampling scheme to support upper-layer sensing applications with dimensionality-consistent CSI, and an incentive strategy that guarantees the sufficiency of CSI. The real-world experimental results demonstrate that *SenCom* is capable of supporting a variety of sensing applications, while retaining good communication performance.

Appendix A
Details for Solving Problem 16

The partial Lagrangian function of problem 16 is given by:

$$\begin{aligned}\mathcal{L} =&\beta\left(\lambda^c[t]+\lambda^i[t]\right)-(1-\beta)\,\Delta\tau[t]\\&+\mu\left(\left(\lambda^c[t]+\lambda^i[t]\right)\mathbb{E}\left\{W\right\}-1+\epsilon\right),\end{aligned}\tag{18}$$

where $\mu \geq 0$ is the Lagrange multiplier associated with the constraint in Eq. 16b. Then, based on the Karush–Kuhn–Tucker conditions, the necessary and sufficient conditions of the optimal solution can be expressed as:

$$\begin{aligned}\frac{\partial\mathcal{L}}{\partial\lambda^i[t]} =&\beta-\frac{(1-\beta)\mathbb{E}\left\{W^2\right\}}{2\left(1-\left(\lambda^c[t]+\lambda^i[t]\right)\mathbb{E}\left\{W\right\}\right)^2}\\&+\mu\mathbb{E}\left\{W\right\}=\begin{cases}=0, & \lambda^i[t]>0,\\ \geq 0, & \lambda^i[t]=0,\end{cases}\end{aligned}\tag{19}$$

$$\mu\left(\left(\lambda^c[t]+\lambda^i[t]\right)\mathbb{E}\left\{W\right\}-1+\epsilon\right)=0.\tag{20}$$

Therefore, there are two cases. (i) When $\lambda^i[t]$ is low and the '=' in Eq. 16b cannot be achieved, we have $\mu=0$ and $\lambda^i[t]$ can be calculated via Eq. 19, as:

$$\lambda^i[t]=\max\left(\frac{1}{\mathbb{E}\left\{W\right\}}\left(1-\sqrt{\frac{1-\beta}{2\beta}\mathbb{E}\left\{W^2\right\}}\right)-\lambda^c[t],0\right).\tag{21}$$

(ii) When $\lambda^i[t]$ is high and the constraint in Eq. 16b limits $\lambda^i[t]$, we have $\mu>0$ and $\lambda^i[t]$ can be calculated via Eq. 20, as:

$$\lambda^i[t]=\frac{1-\epsilon}{\mathbb{E}\left\{W\right\}}-\lambda^c[t].\tag{22}$$

Combining these two cases, we can derive the optimal solution to problem 16, as shown in Eq. 17.

References

[1] Y. He, J. Liu, M. Li, G. Yu, J. Han, and K. Ren, "*SenCom*: Integrated sensing and communication with practical WiFi," in *Proc. Annu. Int. Conf. Mob. Comput. Netw. (MobiCom)*, Oct. 2023, pp. 1–16.

[2] Y. Zheng, Y. Zhang, K. Qian, G. Zhang, Y. Liu, C. Wu, and Z. Yang, "Zero-effort cross-domain gesture recognition with Wi-Fi," in *Proc. Annu. Int. Conf. Mobile Syst. Appl. Services*, Jun. 2019, pp. 313–325.

[3] C. Jiang, J. Guo, Y. He, M. Jin, S. Li, and Y. Liu, "mmVib: micrometer-level vibration measurement with mmwave radar," in *Proc. Annu. Int. Conf. Mob. Comput. Netw. (MobiCom)*, Apr. 2020, pp. 1–13.

[4] W. Xu, J. Liu, S. Zhang, Y. Zheng, F. Lin, J. Han, F. Xiao, and K. Ren, "RFace: Anti-spoofing facial authentication using COTS RFID," in *Proc. IEEE Int. Conf. Comput. Commun. (INFOCOM)*, May 2021, pp. 1–10.

[5] W. Jiang, C. Miao, F. Ma, S. Yao, Y. Wang, Y. Yuan, H. Xue, C. Song, X. Ma, D. Koutsonikolas, W. Xu, and L. Su, "Towards environment independent device free human activity recognition," in *Proc. Annu. Int. Conf. Mob. Comput. Netw. (MobiCom)*, Oct. 2018, pp. 289–304.

[6] Y. Ma, G. Zhou, and S. Wang, "WiFi sensing with channel state information: A survey," *ACM Comput. Surv.*, vol. 52, no. 3, pp. 1–46, Jun. 2019.

[7] I. G. C. Conference, "Workshop on integrated sensing and communication," https://globecom2020.ieee-globecom.org/workshop/ws-05-workshop-integrated-sensing-and-communication-isac, 2020.

[8] I. C. Society, "Integrated sensing and communication," https://www.comsoc.org/publications/journals/ieee-jsac/cfp/integrated-sensing-and-communication, 2021.

[9] B. Bellalta, L. Bononi, R. Bruno, and A. Kassler, "Next generation IEEE 802.11 wireless local area networks: Current status, future directions and open challenges," *Computer Comm.*, vol. 75, pp. 1–25, Feb. 2016.

[10] J. R. Hampton, *Introduction to MIMO communications*. Cambridge university press, 2013.

[11] J. Kim and I. Lee, "802.11 WLAN: history and new enabling MIMO techniques for next generation standards," *IEEE Commun. Mag.*, vol. 53, no. 3, pp. 134–140, Mar. 2015.

[12] C. Wu, X. Huang, J. Huang, and G. Xing, "Enabling ubiquitous WiFi sensing with beamforming reports," in *Proc. ACM SIGCOMM*, Sep. 2023, pp. 20–32.

[13] J. Hu, T. Zheng, Z. Chen, H. Wang, and J. Luo, "MUSE-Fi: Contactless muti-person sensing exploiting near-field Wi-Fi channel variation," in *Proc. Annu. Int. Conf. Mob. Comput. Netw. (MobiCom)*, Oct. 2023, pp. 1–15.

[14] Y. He, G. Yu, Y. Cai, and H. Luo, "Integrated sensing, computation, and communication: System framework and performance optimization," *IEEE Trans. Wireless Commun.*, vol. 23, no. 2, pp. 876–885, Feb. 2024.

[15] R. Fu, S. Mulleti, T. Huang, Y. Liu, and Y. C. Eldar, "Hardware prototype demonstration of a cognitive radar with sparse array antennas," *Electron. Lett.*, vol. 56, no. 22, pp. 1210–1212, Oct. 2020.

[16] F. Liu, C. Masouros, A. Li, H. Sun, and L. Hanzo, "MU-MIMO communications with MIMO radar: From co-existence to joint transmission," *IEEE Trans. Wireless Commun.*, vol. 17, no. 4, pp. 2755–2770, Apr 2018.

[17] X. Liu, T. Huang, N. Shlezinger, Y. Liu, J. Zhou, and Y. C. Eldar, "Joint transmit beamforming for multiuser MIMO communications and MIMO radar," *IEEE Trans. Signal Process.*, vol. 68, pp. 3929–3944, 2020.

[18] Y. He, Y. Cai, H. Mao, and G. Yu, "RIS-assisted communication radar coexistence: Joint beamforming design and analysis," *IEEE J. Sel. Areas Commun.*, vol. 40, no. 7, p. 2131–2145, Jul. 2022.

[19] F. Adib and D. Katabi, "See through walls with WiFi!" in *Proc. ACM SIGCOMM*, Aug. 2013, pp. 75–86.

[20] S. Ji, Y. Xie, and M. Li, "SiFall: Practical online fall detection with RF sensing," in *Proc. Conf. Embed. Networked Sens. (SenSys)*, Nov. 2022, pp. 563–577.

[21] Y. Xu, W. Yang, J. Wang, X. Zhou, H. Li, and L. Huang, "WiStep: Device-free step counting with WiFi signals," *Proc. ACM Interact., Mobile, Wearable Ubiquitous Technol. (IMWUT)*, vol. 1, no. 4, pp. 172:1–172:23, 2017.

[22] Y. Gu, J. Zhan, Y. Ji, J. Li, F. Ren, and S. Gao, "MoSense: An RF-based motion detection system via off-the-shelf WiFi devices," *IEEE Internet Things J.*, vol. 4, no. 6, pp. 2326–2341, Dec. 2017.

[23] S. Li, X. Li, K. Niu, H. Wang, Y. Zhang, and D. Zhang, "AR-Alarm: An adaptive and robust intrusion detection system leveraging CSI from commodity Wi-Fi," in *Proc. Int. Conf. Smart Homes Health Telematics*, Aug. 2017, pp. 211 – 223.

[24] F. Wang, J. Han, F. Lin, and K. Ren, "WiPIN: Operation-free passive person identification using Wi-Fi signals," in *Proc. IEEE Global Commun. Conf.*, Dec. 2019, pp. 1–6.

[25] K. R. Joshi, D. Bharadia, M. Kotaru, and S. Katti, "WiDeo: Fine-grained device-free motion tracing using RF backscatter," in *Proc. USENIX Conf. Netw. Syst. Des. Implementation*, May 2015, pp. 189–204.

[26] H. Abdelnasser, K. A. Harras, and M. Youssef, "UbiBreathe: A ubiquitous non-invasive WiFi-based breathing estimator," in *Proc. ACM Int. Symp. Mobile Ad Hoc Netw. Comput.*, Jun. 2015, pp. 277–286.

[27] I. S. Association *et al.*, "IEEE Std 802.11-2016, IEEE standard for local and metropolitan area networks—part 11: Wireless LAN medium access control (MAC) and physical layer (PHY) specifications," 2016.

[28] D. Tse and P. Viswanath, *Fundamentals of Wireless Communication*. Cambridge university press, 2005.

[29] L. Van der Maaten and G. Hinton, "Visualizing data using t-sne." *J. Mach. Learn. Res.*, vol. 9, no. 11, pp. 2579–2605, 2008.

[30] J. Xiong and K. Jamieson, "Securearray: Improving WiFi security with fine-grained physical-layer information," in *Proc. Annu. Int. Conf. Mob. Comput. Netw. (MobiCom)*, Sep. 2013, pp. 441–452.

[31] Y. Xie, Z. Li, and M. Li, "Precise power delay profiling with commodity WiFi," in *Proc. Annu. Int. Conf. Mob. Comput. Netw. (MobiCom)*, Sep. 2015, pp. 53–64.

[32] M. Grant and S. Boyd, "CVX: Matlab software for disciplined convex programming, version 2.1," 2014.

[33] T. Yoo and A. Goldsmith, "Optimality of zero-forcing beamforming with multiuser diversity," in *Proc. IEEE Int. Conf. Commun. (ICC)*, May 2005, pp. 1–6.

[34] L. D. Nguyen, H. D. Tuan, T. Q. Duong, and H. V. Poor, "Multi-user regularized zero-forcing beamforming," *IEEE Trans. Signal Process.*, vol. 67, no. 11, pp. 2839–2853, Jun. 2019.

[35] Y. Ma, G. Zhou, S. Wang, H. Zhao, and W. Jung, "SignFi: Sign language recognition using WiFi," *Proc. ACM Interact., Mobile, Wearable Ubiquitous Technol. (IMWUT)*, vol. 2, no. 1, pp. 23:1–23:21, Mar. 2018.

[36] S. M. Ross, *Introduction to probability models*. Academic press, 2014.

[37] V. S. Frost and B. Melamed, "Traffic modeling for telecommunications networks," *IEEE Commun. Mag.*, vol. 32, no. 3, pp. 70–81, Mar. 1994.

[38] J. Bi, X. Zhang, H. Yuan, J. Zhang, and M. Zhou, "A hybrid prediction method for realistic network traffic with temporal convolutional network and LSTM," *IEEE Trans Autom. Sci. Eng.*, vol. 19, no. 3, pp. 1869–1879, Jul. 2022.

[39] S. Jachner, K. Gerald van den Boogaart, and T. Petzoldt, "Statistical methods for the qualitative assessment of dynamic models with time delay (R Package qualV)," *J. Stat. Softw.*, vol. 22, no. 8, pp. 1–30, Sep. 2007.

[40] J. Yosinski, J. Clune, Y. Bengio, and H. Lipson, "How transferable are features in deep neural networks?" in *Proc. Adv. Neural Inf. Process. Syst. (NeurIPS)*, Dec. 2014, pp. 3320–3328.

[41] G. Li, S. Wang, J. Li, R. Wang, F. Liu, X. Peng, T. X. Han, and C. Xu, "Integrated sensing and communication from knowledge perspective: An SDP3 approach," *IEEE Internet Things J.*, vol. 11, no. 4, pp. 5589–5603, Feb. 2024.

[42] M. Kotaru, K. Joshi, D. Bharadia, and S. Katti, "SpotFi: Decimeter level localization using WiFi," in *Proc. ACM SIGCOMM*, Aug. 2015, pp. 269–282.

[43] F. Gringoli, M. Schulz, J. Link, and M. Hollick, "Free your CSI: A channel state information extraction platform for modern Wi-Fi chipsets," in *Proc. Int. Workshop Wireless Netw. Testbeds Exp. Eval. Characterization (WiNTECH),*, Oct. 2019, pp. 21–28.

[44] R. Xiao, J. Liu, J. Han, and K. Ren, "OneFi: One-shot recognition for unseen gesture via COTS WiFi," in *Proc. ACM SenSys*, Nov. 2021, pp. 206–219.

[45] M. Müller, "Dynamic time warping," *Inform. Retrieval for Music and Motion.*, pp. 69–84, 2007.

[46] Y. Wang, K. Wu, and L. M. Ni, "WiFall: Device-free fall detection by wireless networks," *IEEE Trans. Mobile Comput.*, vol. 16, no. 2, pp. 581–594, Feb. 2017.

[47] X. Liu, J. Cao, S. Tang, J. Wen, and P. Guo, "Contactless respiration monitoring via off-the-shelf WiFi devices," *IEEE Trans. Mobile Comput.*, vol. 15, no. 10, pp. 2466–2479, Oct. 2016.

Yinghui He (Member, IEEE) received the B.E. degree in information engineering and Ph.D. degree in information and communication engineering from Zhejiang University, Hangzhou, China, in 2018 and 2023, respectively. He is currently a Research Fellow with the College of Computing and Data Science, Nanyang Technological University. His research interests mainly include integrated sensing and communications (ISAC), mobile computing, and device-to-device communications.

Jianwei Liu (Student Member, IEEE) received the BS degree from Northwestern Polytechnical University in 2018 and MS degree from Xi'an Jiaotong University in 2021. He is working toward the Ph.D. degree at Zhejiang University. His research interests include RFID, mobile computing, and smart sensing. He is a student member of the IEEE.

Mo Li (Fellow, IEEE) is a Professor from Hong Kong University of Science and Technology. His research focuses on system aspects of wireless sensing and networking, IoT for smart cities and urban informatics. Dr. Li has been on the editorial board of *IEEE/ACM Transactions on Networking*, *IEEE Transactions on Mobile Computing*, and *IEEE Transactions on Wireless Communications*. He is currently the Editor-in-Chief of *ACM Transactions on Internet of Things*. Dr. Li served the technical program committee member for top conferences in computer system and networking, including ACM MobiCom, ACM MobiSys, IEEE INFOCOM, and many others. Dr. Li is a Distinguished Member of the ACM since 2019, and a Fellow of the IEEE since 2020.

Guanding Yu (Senior Member, IEEE) received the B.E. and Ph.D. degrees in communication engineering from Zhejiang University, Hangzhou, China, in 2001 and 2006, respectively. He joined Zhejiang University in 2006, and is now a Professor with the College of Information and Electronic Engineering. From 2013 to 2015, he was also a Visiting Professor at the School of Electrical and Computer Engineering, Georgia Institute of Technology, Atlanta, GA, USA. His research interests include integrated sensing and communications (ISAC), mobile edge computing/learning, and machine learning for wireless networks.

Dr. Yu has served as a guest editor of IEEE Communications Magazine special issue on Full-Duplex Communications, an Editor of IEEE Journal on Selected Areas in Communications Series on Green Communications and Networking, and Series on Machine Learning in Communications and Networks, an Editor of IEEE Wireless Communications Letters, a lead Guest Editor of IEEE Wireless Communications Magazine special issue on LTE in Unlicensed Spectrum, an Editor of IEEE Transactions on Green Communications and Networking, and an Editor of IEEE Access. He is now serving as an editor of *IEEE Transactions on Machine Learning in Communications and Networking*. He received the 2016 IEEE ComSoc Asia-Pacific Outstanding Young Researcher Award. He regularly sits on the technical program committee (TPC) boards of prominent IEEE conferences such as ICC, GLOBECOM, and VTC. He also serves as a Symposium Co-Chair for IEEE GLOBECOM 2019 and a Track Chair for IEEE VTC 2019'Fall.

Jinsong Han (Senior Member, IEEE) received his Ph.D. degree in computer science from Hong Kong University of Science and Technology in 2007. He is now a professor at the School of Cyber Science and Technology, Zhejiang University. He is a senior member of the ACM and IEEE. His research interests focus on IoT security, smart sensing, wireless and mobile computing.